Cartographic Projection Procedures
Release 4
Second Interim Report

Gerald I. Evenden

September 24, 1995

Contents

1 Release 4.3 Updates. 3

2 Pseudocylindrical Projections. 5
- 2.0.1 Computations. 5
- 2.0.2 Sources. 5
- 2.1 Sinusoidal Pseudocylindricals 5
  - 2.1.1 Generalized Sinusoidal 5
  - 2.1.2 Urmaev Flat-Polar Sinusoidal Series 7
  - 2.1.3 Eckert V 7
  - 2.1.4 Winkel I 7
  - 2.1.5 Wagner III 8
  - 2.1.6 Wagner II 8
  - 2.1.7 Foucaut Sinusoidal. 8
- 2.2 Elliptical Pseudocylindricals. 8
  - 2.2.1 Mollweide, Wagner IV (Putniņš P_2'), and Wagner V 8
  - 2.2.2 Eckert IV 9
  - 2.2.3 Putniņš P_2 9
  - 2.2.4 Hatano 9
  - 2.2.5 Eckert III, Putniņš P_1, Wagner VI (Putniņš P_1'), and Kavraisky VII 10
- 2.3 Hyperbolic Pseudocylindricals 10
  - 2.3.1 Putniņš P_6 and P_6' 10
  - 2.3.2 Putniņš P_5 and P_5' 11
- 2.4 Parabolic Pseudocylindricals 11
  - 2.4.1 Craster (Putniņš P_4) 11
  - 2.4.2 Putniņš P_4' and Werenskiold I . . 11
  - 2.4.3 Putniņš P_3 and P_3' 12
  - 2.4.4 McBryde-Thomas Flat-Polar Parabolic 12
- 2.5 Rectilinear 12
  - 2.5.1 Collignon 12
  - 2.5.2 Eckert I 12
  - 2.5.3 Eckert II 13
- 2.6 Miscellaneous pseudo/Pseudocylindricals. 13
  - 2.6.1 Sine-Tangent Series 13
  - 2.6.2 McBryde-Thomas Flat-Polar Sine (No. 1). 13
  - 2.6.3 McBryde-Thomas Flat-Polar Quartic 14
  - 2.6.4 Boggs Eumorphic 14
  - 2.6.5 Nell-Hammer 14
  - 2.6.6 Robinson 14
  - 2.6.7 Denoyer 15
  - 2.6.8 Fahey 15
  - 2.6.9 Ginsburg VIII or TsNIIGAiK . . 15
  - 2.6.10 Loximuthal 15
  - 2.6.11 Winkel II 16
  - 2.6.12 Urmaev V Series 16
  - 2.6.13 Goode Homolosine 16

3 Miscellaneous Projections. 17
- 3.1 Near Pseudocylindricals. 17
  - 3.1.1 Aitoff 17
  - 3.1.2 Winkel Tripel 17
  - 3.1.3 Hammer (Hammer-Aitoff) and Eckert-Greifendorff. 17
  - 3.1.4 Larrivée. 17
  - 3.1.5 Wagner VII. 17
  - 3.1.6 Laskowski. 18

4 Creating Oblique Projections. 19

1 Release 4.3 Updates.

As with the previous Rel. 4 update manual, this represents new changes reflected in the third subrelease. The main reason for not combining this material with updates in the previous report in one document are the changes in typesetting style and the delays that would be caused with changing style in the previous report.

Changes most obvious to users of the program **proj** are the addition of new projections—the total is now about 110. For programmers using the projection library, the main change is in how to limit the list of projections linked into application programs. Additional, internal changes were made to ease maintenance of the system, but they should be transparent to both user and programmer.

Manual Style. This update is concerned with only documenting projections. Waffling by the author about what should be included or ignored are beginning to converge to the style presented here. Description of the Pseudocylindrical class of projections that follows is nearly complete and will probably not change greatly in the final documentation. A few of previous Miscellaneous projections and new additions are included as well as a section on the General Oblique projection.

It was also decided to include the formulary as part of documentation for reference by the serious reader and to make an explicit definition of what is considered by the author to be the mathematical definition of each projection in this system.

Any comments as to this new style are appreciated.

Apologies. Because automatic typesetting programs do not always make the best choices, there are several undesirable locating of figures relative to text. These can usually be overcome by extra effort by the author, but such manipulations are likely to be destroyed by later, overall document alterations. Thus, little effort was expended at this preliminary stage in "beautifying" the text.

2 Pseudocylindrical Projections.

Pseudocylindrical projections are a result of efforts to minimize the distortion of the polar regions of the cylindrical projections by bending the meridians toward the center of the map as a function of longitude while maintaining the cylindrical characterstic of parallel parallels. These projections are almost excusively used for small scale global displays and, except for the Sinsoidal projection, only derived for a spherical Earth. Because of the basic definition of pseudocylindrical projections, none are conformal, but many are equal area.

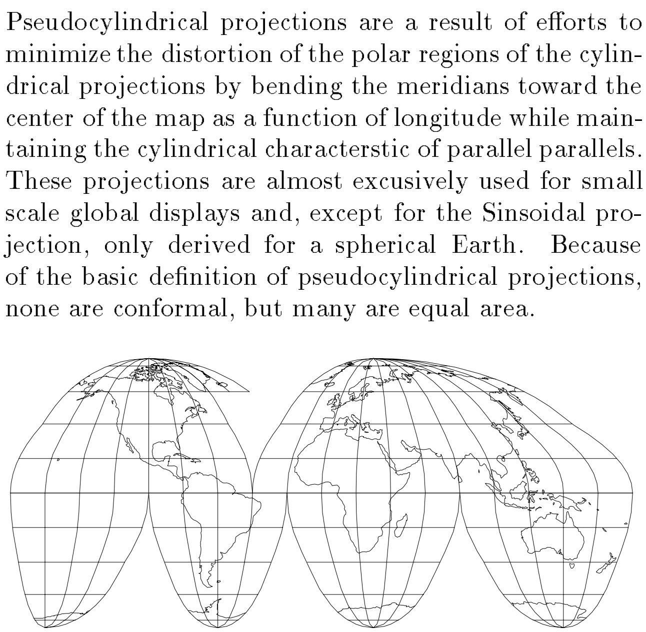

Figure 1: Interupted Goode Homolosine emphasizing land masses.

To further reduce distortion, pseudocylindrical are often presented in interupted form that are made by joining several regions with appropriate central meridians and false easting and clipping boundaries. Figs. 1 and 2 show typical construction that are suited for showing respective global land and oceanic regions. To reduce the lateral size of the map, some uses remove an irregular, North-South strip of the mid-Atlantic region so that the western tip of Africa is plotted north of the eastern tip of South America.

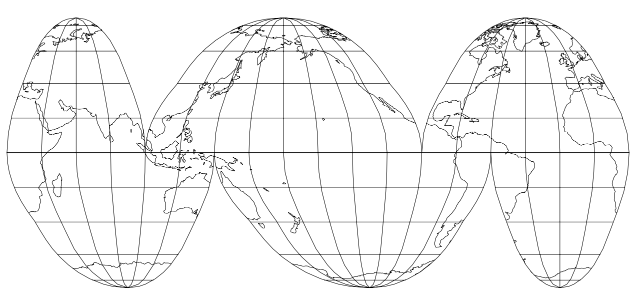

Figure 2: Interupted Goode Homolosine emphasizing oceanic masses.

Pseudocylindrical are sub-classed into groups based upon the shape of the merdians: sinusoidal, elliptical, parabolic, hyperbolic, rectilinear and miscellaneous. An additional category is based upon whether the meridians come to a point at the pole or are terminated along a straight line—flat-topped.

2.0.1 Computations.

A complicating factor in computing the forward projection for pseudocylindricals is that some of the projection formulae use a parametric variable, typically θ, which is a function of ϕ. In some cases, the parametric equation is not directly solvable for θ and requires use of Newton-Raphson's method of iterative finding the root of $P(\theta)$. The defining equations for these cases are thus given in the form of $P(\theta)$ and its derivative, $P'(\theta)$, and an estimating initial value for $\theta_0 = f(\phi)$. Refinement of θ is made by $\theta \leftarrow \theta - P(\theta)/P'(\theta)$ until $|P(\theta)/P'(\theta)|$ is less than predefined tolerance.

When known, formula constant factors are given in rational form (e.g. $\sqrt{2}/2$) rather than a decimal value (0.7071) so that the precision used in the resultant program code constants is determined by the programmer. However, source material may only provide decimal values, typically to 5 or 6 decimal digits. This is adequate in most cases, but has caused problems with the convergence of a Newton-Raphson determination and degrades the determination of numerical derivatives.

Because several of the pseudocylindrical projections have a common computational base, they are grouped into a single module with multiple initializing entry points. This may lead to a minor loss of efficiency, such as adding a zero term in the simple Sinusoidal case of the the Generalized Sinusoidal (2.1.1).

2.0.2 Sources.

The principle source for pseudocylindrical formulae is [7]. Many formulae are repeated in Snyder's later works [11] and [10], with the latter adding a few additional projections. Mahling, [2], covers several of the Russian projections but the formulae are often difficult to read. Mahling also has given fourteen pseudocylindrical formulae in [3, Appendix 1] but some discrepancies are found when compared to Snyder's work. For the Robinson Projection (2.6.6), [6] was consulted to verify precision of tabular values and lack of specification of interpolation method. Common pseudocylindicals formulae are also found in Pearson's work: [4] and [5]. Ellipsoid formulae for the Sinusoidal projection is from [9].

2.1 Sinusoidal Pseudocylindricals

2.1.1 Generalized Sinusoidal

McBryde and Thomas developed a generalized formulas for several of the pseudocylindricals with sinusoidal meridians:

$$\begin{aligned} x &= C\lambda(m + \cos\theta)/(m+1) \\ y &= C\theta \\ C &= \sqrt{(m+1)/n} \end{aligned}$$

Table 1: List of pseudocylindrical projections

Projection name	Fig.	Class	Sect.	H/V	P/H	`+proj=`	args	file
Boggs Eumorphic	39	A,M	2.6.4	2	0	`boggs`		`boggs.c`
Collignon	30	A,R	2.5.1	2	0	`collg`		`collg.c`
Craster (Putniņš P_4)	24	A,P	2.4.1	2	0	`crast`		`crast.c`
Denoyer	42	M	2.6.7	2	0.3075	`denoy`		`denoy.c`
Eckert I	31	R	2.5.2	2	1/2	`eck1`		`eck1`
II	32	A,R	2.5.3	2	1/2	`eck2`		`eck2`
III	16	E	2.2.5	2	1/2	`eck3`		`eck3.c`
IV	13	A,E	2.2.2	2	1/2	`eck4`		`eck4.c`
V	5	S	2.1.3	2	1/2	`eck5`		`eck5.c`
VI	3	A,S	2.1.1	2	1/2	`eck6`		`gn_sinu.c`
Fahey	43	M	2.6.8	1.4146	0	`fahey`		`fahey.c`
Foucaut	36	A,S	2.6.1	1.5708	0	`fouc`		`sts.c`
Foucaut Sinusoidal	9	A,M	2.1.7	1.5708	0	`fouc_s`		`fouc_s.c`
General Sinusoidal		S	2.1.1			`gn_sinu`	`+n= +m=`	`gn_sinu.c`
Ginsburg VIII	44	M	2.6.9	1.2893	0.5993	`gins8`		`gins8.c`
Goode Homolosine	47	A,M	2.6.13	2.3076	0	`goode`		`goode`
Hatano	15	A,E	2.2.4	2.0372	1/3	`hatano`		`hatano`
Kavraisky VII	19	E	2.2.5	$\sqrt{3}$	1/2	`kav7`		`eck3.c`
V	35	A,M	2.6.1	2.0495	0	`kav5`		`sts.c`
Loximuthal	45	M	2.6.10			`loxim`	`+lat_1=`	`loxim.c`
McBryde-Thomas								
Sine (No. 1)	34	A,M	2.6.1	2.1192	0	`mbt_s`		`sts.c`
Flat-Polar Sine (No. 2)	37	A,M	2.6.2	2.1192	0	`mbt_fps`		`mbt_fps.c`
Flat-Polar Sinusoidal (No. 3)	3	A,S	2.1.1	2	1/3	`mbtfps`		`gn_sinu.c`
Flat-Polar Quartic (No. 4)	38	A,M	2.6.3	2.2214	1/3	`mbtfpq`		`mbtfpq`
Flat-Polar Parabolic (No. 5)	29	A,P	2.4.4	2.0944	1/3	`mbtfpp`		`mbtfpp.c`
Mollweide	10	A,E	2.2.1	2	0	`moll`		`moll.c`
Putniņš P_1	17	E	2.2.5	2	0	`putp1`		`eck3.c`
P_2	14	A,E	2.2.3	2	0	`putp2`		`putp2.c`
P_3	27	P	2.4.3	2	0	`putp3`		`putp3.c`
P_3'	28	P	2.4.3	2	1/2	`putp3p`		`putp3.c`
P_4'	25	A,P	2.4.2	2	1/2	`putp4p`		`putp4p.c`
P_5	22	H	2.3.2	2	0	`putp5`		`putp5.c`
P_5'	23	H	2.3.2	2	1/2	`putp5p`		`putp5.c`
P_6	20	H,E	2.3.1	2	0	`putp6`		`putp6.c`
P_6'	20	H,E	2.3.1	2	1/2	`putp6p`		`putp6.c`
Nell-Hammer	40	A,M	2.6.5	2.7519	1/2	`nell_h`		`nell_h.c`
Quartic Authalic	33	A,M	2.6.1	2.2214	0	`qua_aut`		`sts.c`
Robinson	41	M	2.6.6	1.9717	0.5322	`robin`		`robin.c`
Sinusoidal	3	A,S	2.1.1	2	0	`sinu`		`gn_sinu.c`
Urmaev Flat-Polar Sinusoidal		A,S	2.1.2		$\sqrt{1-n^2}$	`urmfps`	`+n=`	`urmfps.c`
V Series		A,M	2.6.12			`urm5`	`+n= +q= +alpha=`	`urm5.c`
Wagner I (Kavraisky VI)	4	A,S	2.1.2	2	1/2	`wag1`		`urmfps.c`
II	8	S	2.1.6	2	1/2	`wag2`		`wag2.c`
III	7	S	2.1.5			`wag3`	`+lat_ts=`	`wag3.c`
IV (Putniņš P_2')	11	A,E	2.2.1	2	1/2	`wag4`		`moll.c`
V	12	S	2.2.1	1.9429	0.4531	`wag5`		`moll.c`
VI (Putniņš P_1')	18	E	2.2.5	2	1/2	`wag6`		`putp1peck3.c`
Werenskiold	26	A,H	2.4.2	2	1/2	`weren`		`putp4p.c`
Winkel I	46	S	2.1.4	2	1/2	`wink1`	`+lat_ts=`	`wink1.c`
Winkel II	46	M	2.6.11			`wink2`	`+lat_1=`	`wink2.c`

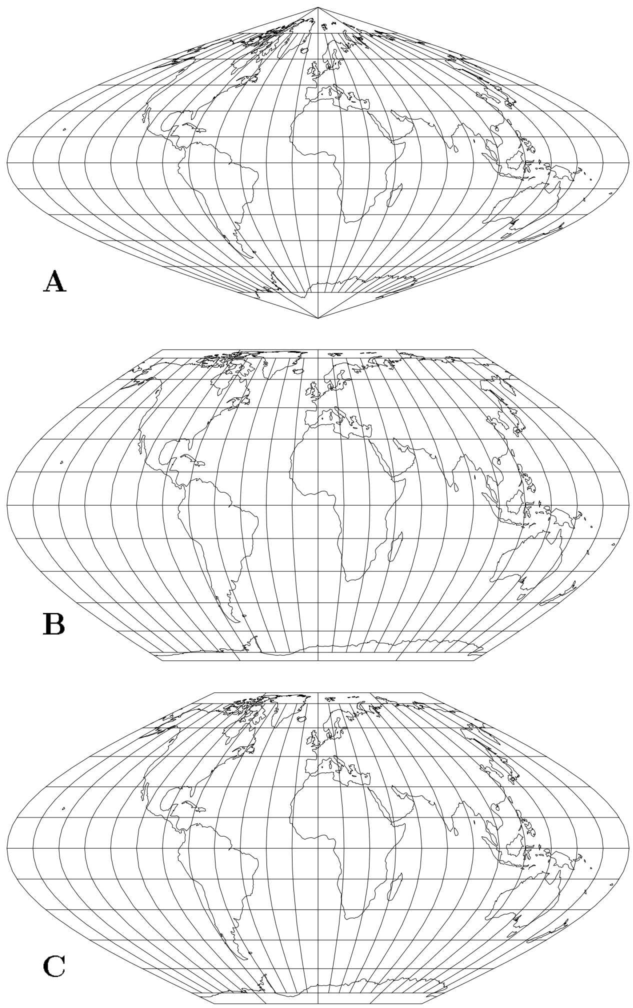

Figure 3: Sinusoidal projections from general formulas: **A**–Sinusoidal, **B**–Eckert VI and **C**–McBryde-Thomas Flat-Polar Sinusoidal.

$$
\begin{aligned}
P(\theta) &= m\theta + \sin\theta - n\sin\phi \\
P'(\theta) &= m + cos\theta \\
\theta_0 &= \phi
\end{aligned}
$$

	m	n	C
Sinusoidal (Sanson-Flamsteed)	0	1	1
Eckert VI	1	$1+\pi/2$	$2/\sqrt{2+\pi}$
McBryde-Thomas Flat-Polar Sinusoidal	1/2	$1+\pi/4$	$\sqrt{6/(4+\pi)}$

Parameters `n=`n and `m=`m are required for the general form, `proj=gn_sinu`. The projection is equal-area for all cases.

When $m = 0$, $P(\theta)$ simplifies and does not need Newton-Raphson iterative solution and in the Sinusoidal case, $\theta = \phi$.

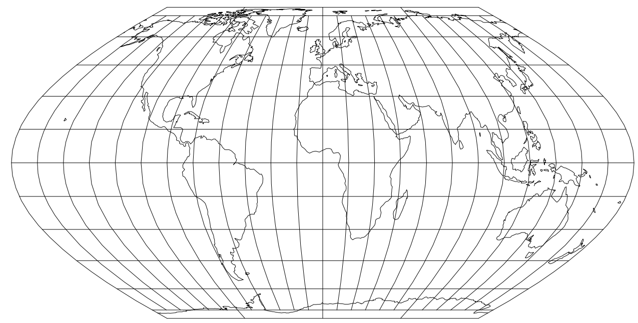

Figure 4: Wagner I.

Elliptical Earth. The Sinusoidal projection for the ellipsoidal case becomes:

$$
\begin{aligned}
x &= \lambda\cos\phi(1 - e^2\sin^2\phi)^{-1/2} \\
y &= \mathrm{M}(\phi)
\end{aligned}
$$

The inverse is readily solved by determining ϕ from $\mathrm{M}^{-1}(y)$ and substituting into the x equation for the solution of λ.

2.1.2 Urmaev Flat-Polar Sinusoidal Series

This equal-area system is similar to 2.1.1 where the respective x and y axis are multiplied and divided by $\sqrt{2/3}$ and where $m = 0$. The parameter, `n=`n, must be specified and is restricted by $0 < n \leq 1$. The Wagner I (Kavraisky VI) projection is generated when `n=`$\sqrt{3}/2$ or by selecting `proj=wag1`.

$$
\begin{aligned}
x &= (2\sqrt[4]{3}/3)\lambda\cos\theta \\
y &= 3\theta/(2n\sqrt[4]{3}) \\
\sin\theta &= n\sin\phi
\end{aligned}
$$

Latitude of true scale on the central meridian is determined by the relation: $\sin^2\phi_{ts} = (9-4\sqrt{3})/(9-4n^2\sqrt{3})$. The ratio of the length of the poles to the equator is determined by $\sqrt{1-n^2}$.

2.1.3 Eckert V

$$
\begin{aligned}
x &= \lambda(1+\cos\phi)/\sqrt{2+\pi} \\
y &= 2\phi/\sqrt{2+\pi}
\end{aligned}
$$

2.1.4 Winkel I

Option `lat_ts=`ϕ_{ts} estabishes latitude of true scale on central meridian (default = $0°$ and thus the same as Eckert V). Not equal-area but if $\cos\phi_{ts} = 2/\pi$ (`lat_ts=50d28'`) the total area of the global map is correct. If $\phi_{ts} = 0$

$$
\begin{aligned}
x &= \lambda(\cos\phi_{ts} + \cos\phi)/2 \\
y &= \phi
\end{aligned}
$$

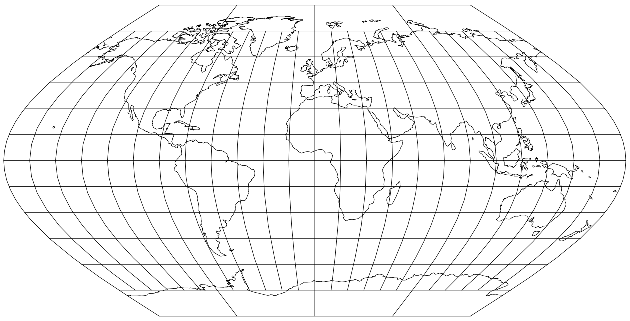

Figure 5: Eckert V.

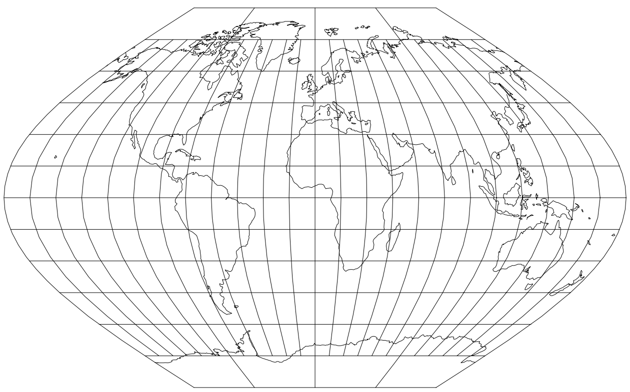

Figure 6: Winkel I, `lat_ts=50d28'`

2.1.5 Wagner III

$$
\begin{aligned}
x &= [\cos\phi_{ts}/\cos(2\phi_{ts}/3)]\lambda\cos(2\phi/3) \\
y &= \phi
\end{aligned}
$$

2.1.6 Wagner II

$$
\begin{aligned}
x &= 0.92483\lambda\cos\theta \\
y &= 1.387254\theta \\
\sin\theta &= 0.88022\sin(0.8855\phi)
\end{aligned}
$$

2.1.7 Foucaut Sinusoidal.

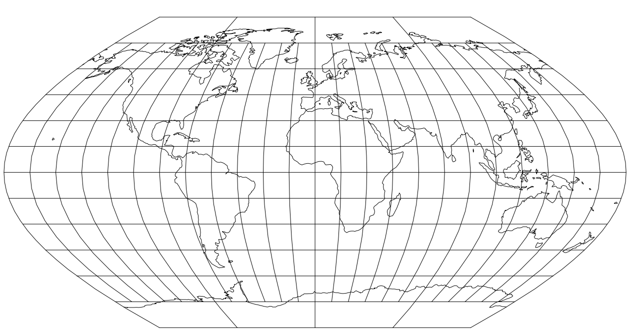

Figure 7: Wagner III.

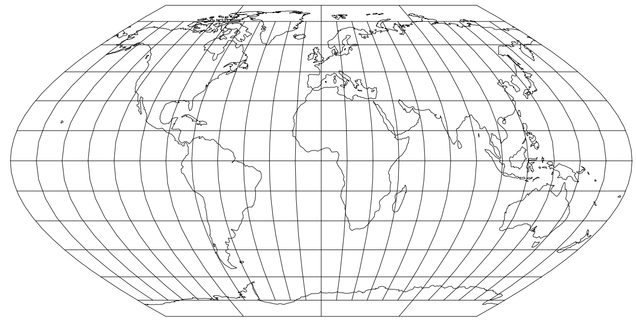

Figure 8: Wagner II.

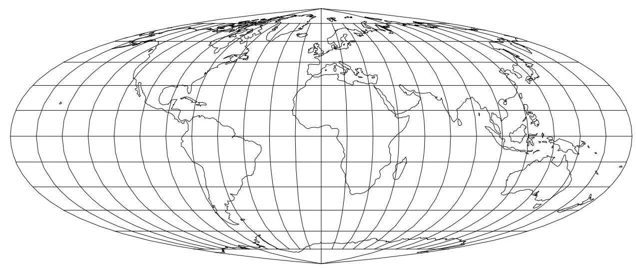

Figure 9: Foucaut Sinusoidal, `+n=0.5`.

The y-axis is based upon a weighted mean of the cylindrical equal-area and the sinusoidal projections. Parameter `n=`n is the weighting factor where $0 \le n \le 1$.

$$
\begin{aligned}
x &= \lambda\cos\phi/(n + (1-n)\cos\phi) \\
y &= n\phi + (1-n)\sin\phi
\end{aligned}
$$

For the inverse, the Newton-Raphson method can be used to determine ϕ from the equation for y above. As $n \to 0$ and $\phi \to \pi/2$, convergence is slow but for $n = 0$, $\phi = \sin^{-1} y$.

2.2 Elliptical Pseudocylindricals.

2.2.1 Mollweide, Wagner IV (Putniņš P_2'), and Wagner V

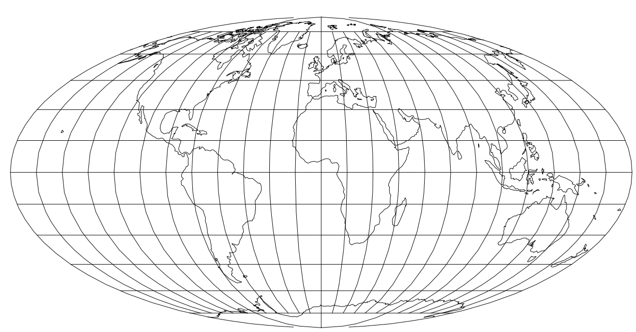

Figure 10: Mollweide.

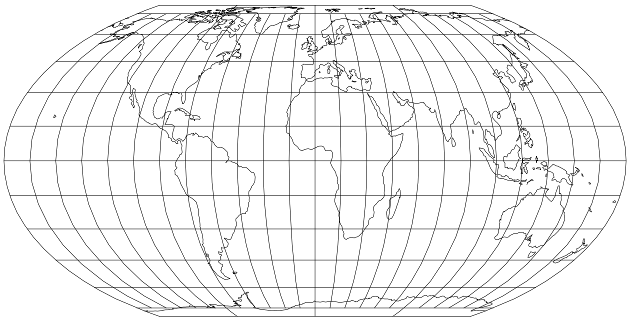

Figure 11: Wagner IV.

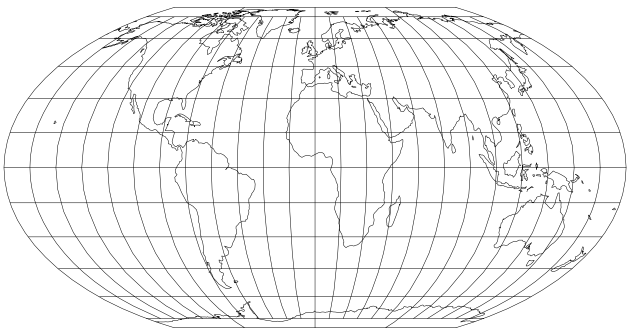

Figure 12: Wagner V

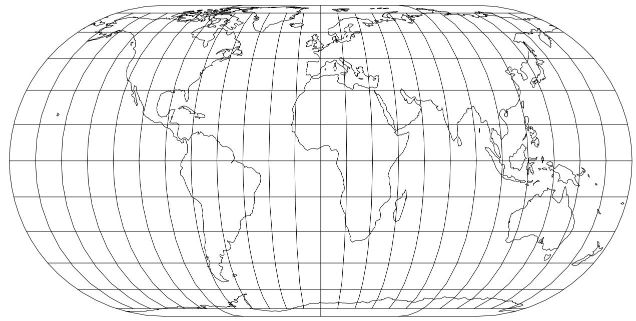

Figure 13: Eckert IV.

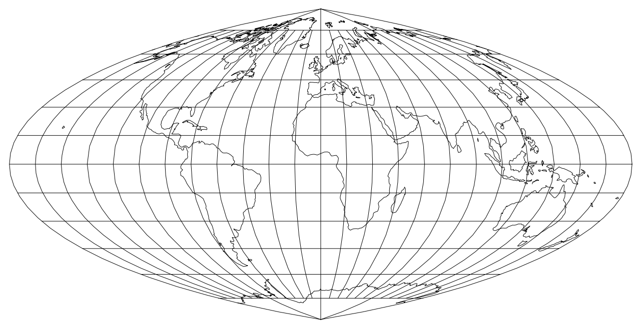

Figure 14: Putniņš P_2.

Mollweide and Wagner IV are equal area, but Wagner V is not.

$$
\begin{aligned}
x &= C_x \lambda \cos(\theta/2) \\
y &= C_y \sin(\theta/2) \\
C_x &= 0.90977 \quad \text{for Wagner V} \\
&= 2r/\pi \quad \text{otherwise} \\
C_y &= 1.65014 \quad \text{for Wagner V} \\
&= r/\sin p \quad \text{otherwise} \\
P(\theta) &= \theta + \sin\theta - C_p \sin\phi \\
C_p &= 3.00896 \quad \text{for Wagner V} \\
&= 2p + \sin 2p \quad \text{otherwise} \\
P'(\theta) &= 1 + \cos\theta \\
\theta_0 &= \phi \\
r &= \sqrt{2\pi \sin p/(2p + \sin 2p)}
\end{aligned}
$$

and where $p = \pi/2$ for Mollweide and $p = \pi/3$ for Wagner IV. The parametric equation converges slowly for the Mollweide case.

2.2.2 Eckert IV

$$
\begin{aligned}
x &= 2\lambda(1 + \cos\theta)/\sqrt{\pi(4+\pi)} \\
y &= 2\sqrt{\pi/(4+\pi)}\sin\theta \\
P(\theta) &= \theta + \sin 2\theta + 2\sin\theta - \frac{(4+\pi)}{2}\sin\phi \\
&= \theta + \sin\theta(\cos\theta + 2) - \frac{(4+\pi)}{2}\sin\phi \\
P'(\theta) &= 2 + 4\cos 2\theta + 4\cos\theta \\
&= 1. + \cos\theta(\cos\theta + 2) - \sin^2\theta \\
\theta_0 &= 0.895168\phi + 0.0218849\phi^3 + 0.00826809\phi^5
\end{aligned}
$$

2.2.3 Putniņš P_2

$$
\begin{aligned}
x &= 1.89490\lambda(\cos\theta - 1/2) \\
y &= 1.71848\sin\theta \\
P(\theta) &= 2\theta + \sin 2\theta - 2\sin\theta - [(4\pi - 3\sqrt{3})/6]\sin\phi \\
&= \theta + \sin\theta(\cos\theta - 1) - [(4\pi - 3\sqrt{3})/12]\sin\phi \\
P'(\theta) &= 2 + 2\cos 2\theta + 2\cos\theta \\
&= 1 + \cos\theta(\cos\theta - 1) - \sin^2\theta \\
\theta_0 &= 0.615709\phi + 0.00909953\phi^3 + 0.0046292\phi^5
\end{aligned}
$$

The parametric equation converges slowly as ϕ nears $\pi/2$ and θ approaches $pi/3$.

2.2.4 Hatano

$$
\begin{aligned}
x &= 0.85\lambda\cos\theta \\
y &= C_y \sin\theta \\
P(\theta) &= 2\theta + \sin 2\theta - C_p \sin\phi \\
P'(\theta) &= 2(1 + \cos 2\theta) \\
\theta_0 &= 2\phi
\end{aligned}
$$

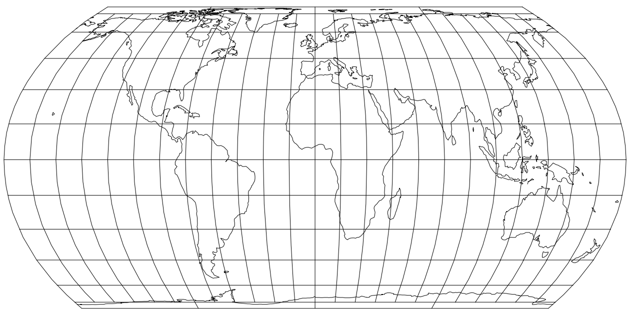

Figure 15: Hatano.

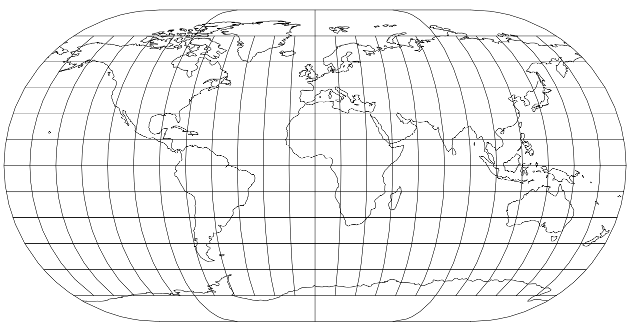

Figure 16: Eckert III.

	C_y	C_p
$\phi > 0$	1.75859	2.67595
$\phi < 0$	1.93052	2.43763

For $\phi = 0$, $y \leftarrow 0$ and $x \leftarrow 0.85\lambda$.

2.2.5 Eckert III, Putniņš $\mathbf{P}_1$, Wagner VI (Putniņš $\mathbf{P}'_1$), and Kavraisky VII

None of these projections are equal-area and are flat-polar when coefficient $A \neq 0$.

$$
\begin{aligned}
x &= C_x\lambda(A + \sqrt{1 - B(\phi/\pi)^2}) \\
y &= C_y\phi
\end{aligned}
$$

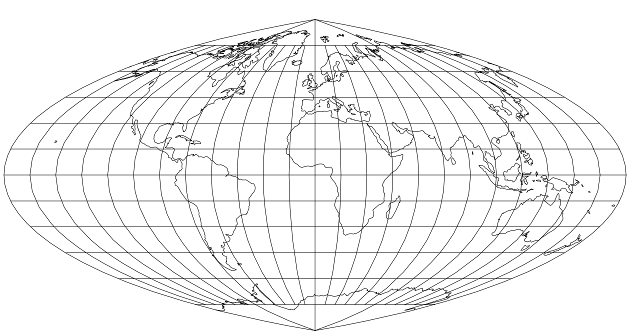

Figure 17: Putniņš P_1.

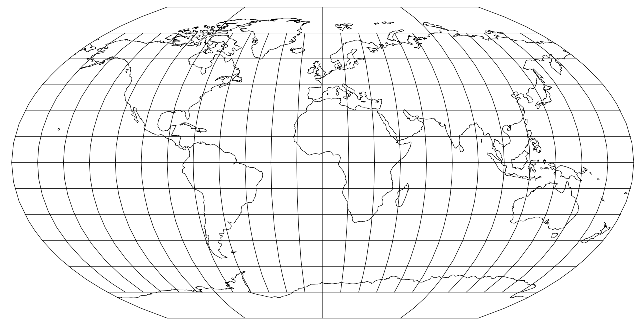

Figure 18: Wagner VI.

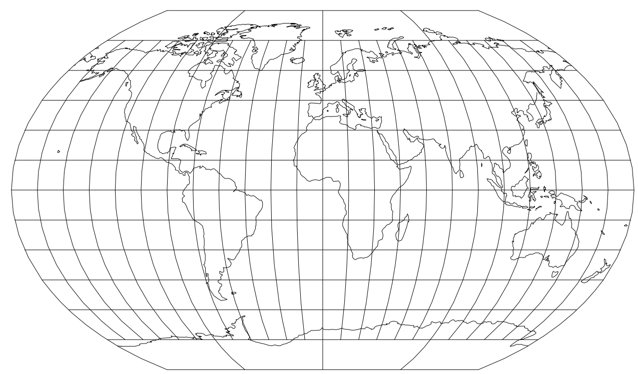

Figure 19: Kavraisky VII.

	C_x	C_y	A	B
Putniņš P_1	0.94745	0.94745	0	3
Wagner VI	1.89490	0.94745	$-1/2$	3
Eckert III	$\frac{2}{\sqrt{\pi(4+\pi)}}$	$\frac{4}{\sqrt{\pi(4+\pi)}}$	1	4
Kavraisky VII	$\sqrt{3}/2$	1	0	3

2.3 Hyperbolic Pseudocylindricals

In this group where the meridians are hyperbolic only four Putniņš forms are given.

2.3.1 Putniņš $\mathbf{P}_6$ and $\mathbf{P}'_6$

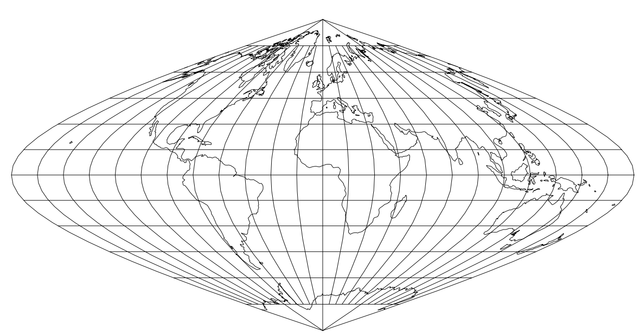

Figure 20: Putniņš P_6.

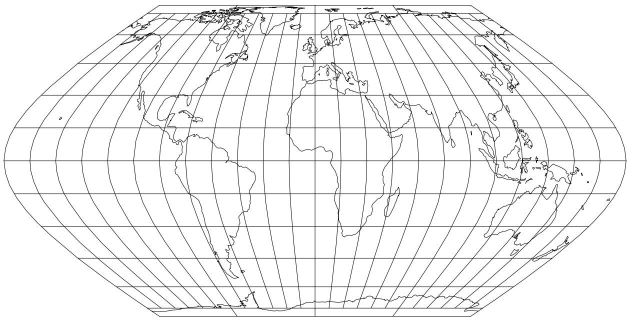

Figure 21: Putniņš P'_6.

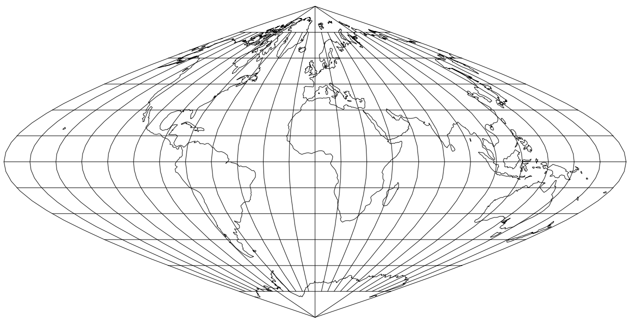

Figure 22: Putniņš P_5.

Putniņš P_6 and P'_6 projections are equal-area with respective pointed and flat poles defined by:

$$
\begin{aligned}
x &= C_x\lambda(D-(1+p^2)^{1/2}) \\
y &= C_y p \\
P(p) &= (A-(1+p^2)^{1/2})p - \ln(p+(1+p^2)^{1/2}) \\
&\quad -B\sin\phi \\
P'(p) &= A - 2\sqrt{1+p^2} \\
p_0 &= \phi
\end{aligned}
$$

where

	P_6	P'_6
C_x	1.01346	0.44329
D	2	3
C_y	0.91910	0.80404
A	4.00000	6.00000
B	2.14714	5.61125

2.3.2 Putniņš P_5 and P'_5

Putniņš P_5 and P'_5 projections have equally spaced parallels and respectively pointed and flat poles:

$$
\begin{aligned}
x &= 1.01346\lambda(A - B\sqrt{1+12\phi^2/\pi^2}) \\
y &= 1.01346\phi
\end{aligned}
$$

	P_5	P'_5
A	2.0	1.5
B	1.0	0.5

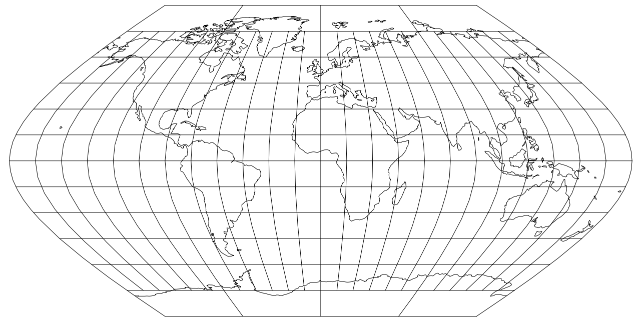

Figure 23: Putniņš P'_5.

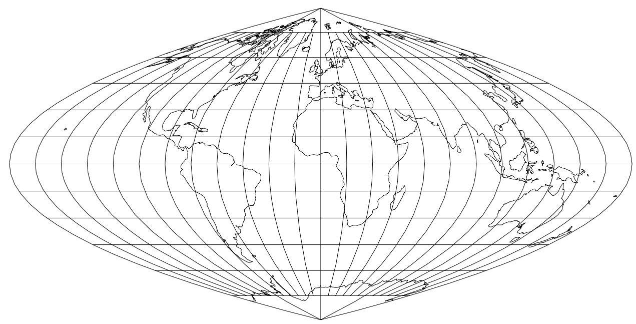

Figure 24: Craster.

2.4 Parabolic Pseudocylindricals

In this group where the meridians are parabolic.

2.4.1 Craster (Putniņš P_4)

A pointed pole, equal-area projection with standard parallels at 36°46′.

$$
\begin{aligned}
x &= \sqrt{3/\pi}\lambda[2\cos(2\phi/3)-1] \\
y &= \sqrt{3\pi}\sin(\phi/3)
\end{aligned}
$$

2.4.2 Putniņš P'_4 and Werenskiold I

This is the flat pole version of Putniņš's P_4 or Craster's Parabolic:

$$
x = C_x\lambda\cos\theta/\cos(\theta/3)
$$

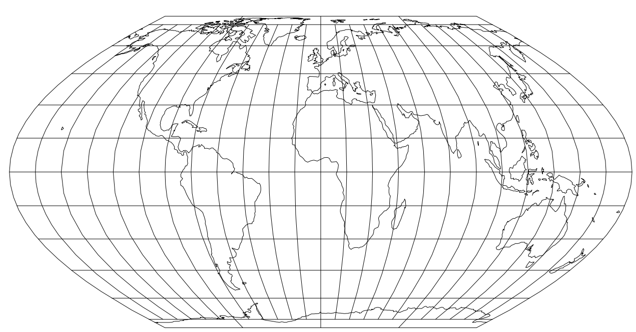

Figure 25: Putniņš P'_4.

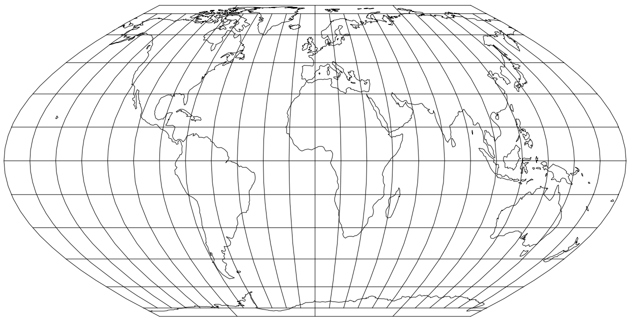

Figure 26: Werenskiold I.

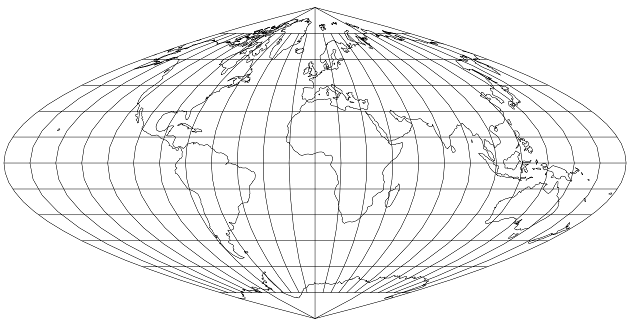

Figure 27: Putniņš P_3.

$$
\begin{aligned}
y &= C_y \sin(\theta/3) \\
\sin\theta &= (5\sqrt{2}/8)\sin\phi
\end{aligned}
$$

where

	P'_4	Weren. I
C_x	$2\sqrt{0.6/\pi}$	1.0
C_y	$2\sqrt{1.2\pi}$	$\pi\sqrt{2}$

2.4.3 Putniņš P_3 and P'_3

$$
\begin{aligned}
x &= \sqrt{2/\pi}\lambda(1 - A\phi^2/\pi^2) \\
y &= \sqrt{2/\pi}\phi
\end{aligned}
$$

where A is 4 and 2 for respective P_3 and P'_3.

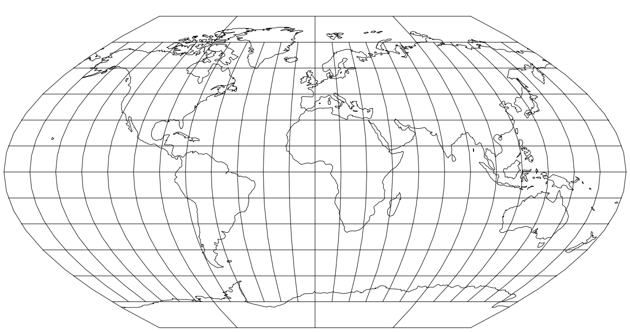

Figure 28: Putniņš P'_3.

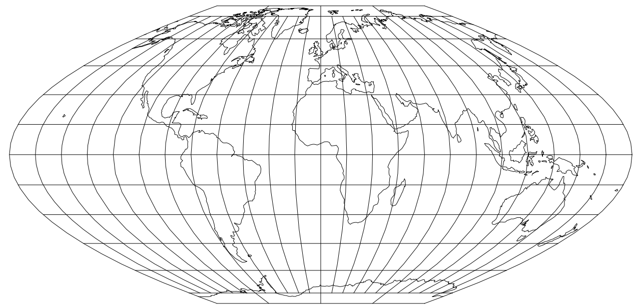

Figure 29: McBryde-Thomas Flat-Polar Parabolic.

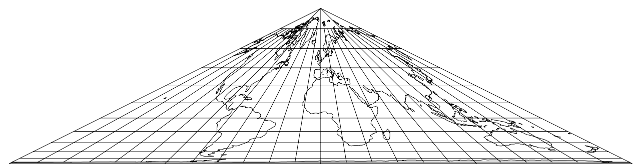

Figure 30: Collignon.

2.4.4 McBryde-Thomas Flat-Polar Parabolic

$$
\begin{aligned}
x &= \sqrt{6/7}/3\lambda[1 + 2\cos\theta/\cos(\theta/3)] \\
y &= 3\sqrt{6/7}\sin(\theta/3) \\
P(\theta) &= 1.125\sin(\theta/3) - \sin^3(\theta/3) - 0.4375\sin\phi \\
P'(\theta) &= [0.375 - \sin^2(\theta/3)]\cos(\theta/3) \\
\theta_0 &= \phi
\end{aligned}
$$

2.5 Rectilinear

2.5.1 Collignon

$$
\begin{aligned}
x &= (2/\sqrt{\pi})\lambda\sqrt{1 - \sin\phi} \\
y &= \sqrt{\pi}(1 - \sqrt{1 - \sin\phi})
\end{aligned}
$$

2.5.2 Eckert I

$$
\begin{aligned}
x &= 2\sqrt{2/3\pi}\lambda(1 - |\phi|/\pi) \\
y &= 2\sqrt{2/3\pi}\phi
\end{aligned}
$$

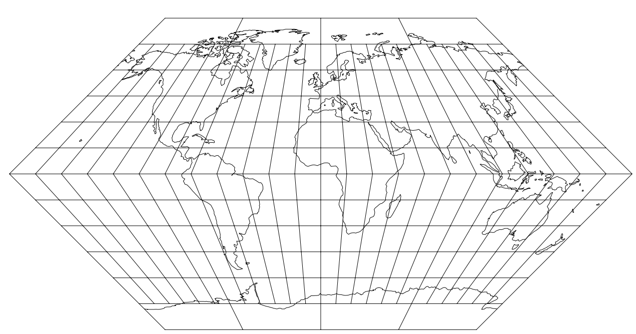

Figure 31: Eckert I.

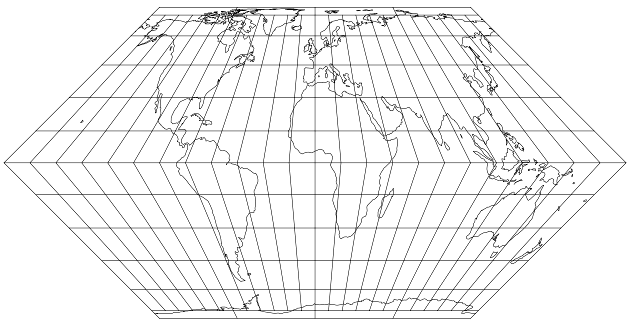

Figure 32: Eckert II.

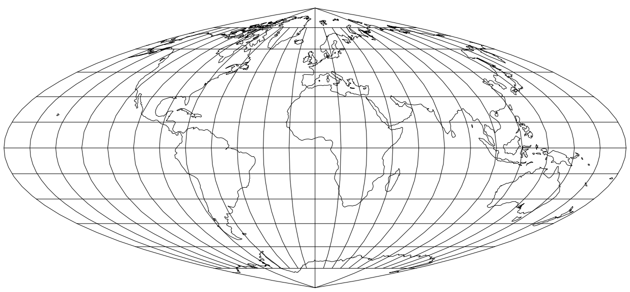

Figure 33: Quartic Authalic.

2.5.3 Eckert II

$$
\begin{aligned}
x &= (2/\sqrt{6\pi})\lambda\sqrt{4 - 3\sin|\phi|} \\
y &= \sqrt{2\pi/3}(2 - \sqrt{4 - 3\sin|\phi|}) \\
& \quad y \text{ assumes sign of } \phi
\end{aligned}
$$

2.6 Miscellaneous pseudo/Pseudocylindricals.

2.6.1 Sine-Tangent Series

Sine series:

$$
\begin{aligned}
x &= (q/p)\lambda\cos\phi/\cos(\phi/q) \\
y &= p\sin(\phi/q)
\end{aligned}
$$

Tangent series:

$$
\begin{aligned}
x &= (q/p)\lambda\cos\phi\cos^2(\phi/q) \\
y &= p\tan(\phi/q)
\end{aligned}
$$

q	p	Sine	Tangent
2	2	Quartic Authalic	Foucaut
1.36509	1.48875	McBryde-Thomas	
1.35439	1.50488	Kavraisky V	

2.6.2 McBryde-Thomas Flat-Polar Sine (No. 1).

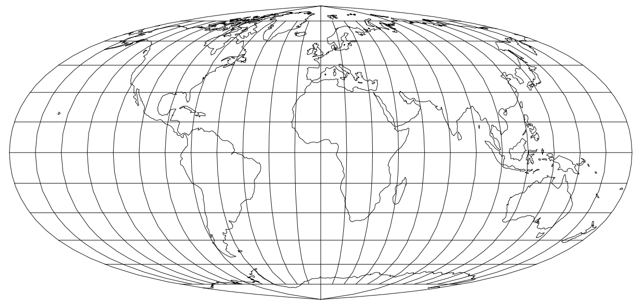

Figure 34: McBryde-Thomas Sine.

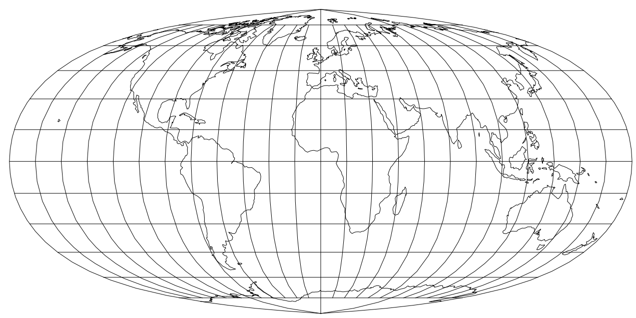

Figure 35: Kavraisky V.

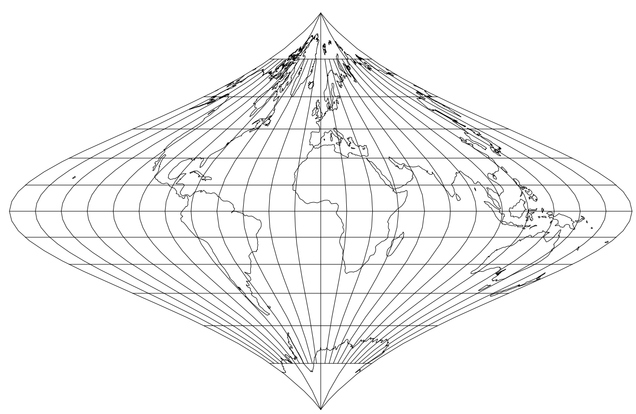

Figure 36: Foucaut.

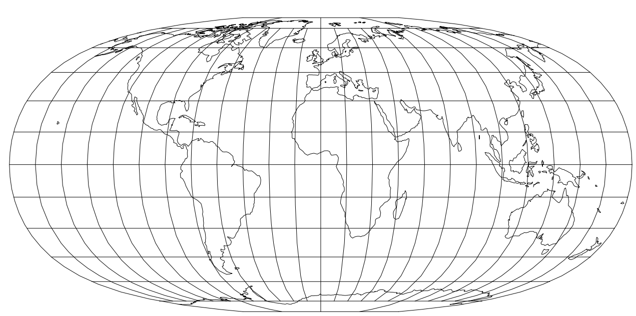

Figure 37: McBryde-Thomas Flat-Polar Sine (No. 1).

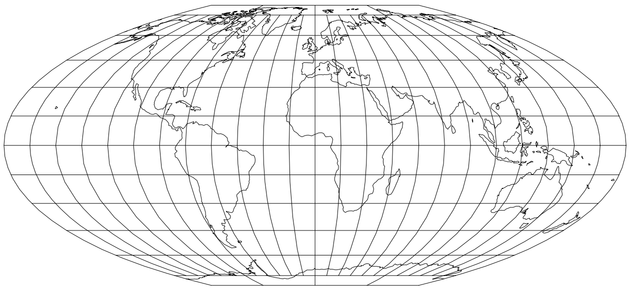

Figure 38: McBryde-Thomas Flat-Polar Quartic.

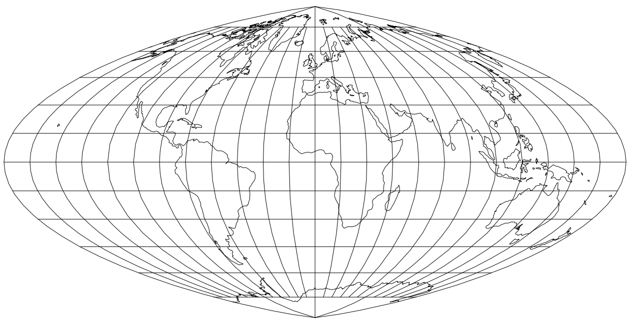

Figure 39: Boggs Eumorphic.

$$
\begin{aligned}
x &= 0.22248\lambda[1 + 3\cos\theta/\cos(\theta/1.36509)] \\
y &= 1.44492\sin(\theta/1.36509) \\
P(\theta) &= 0.45503\sin(\theta/1.36509) + \sin\theta - 1.41546\sin\phi \\
P'(\theta) &= \frac{0.45503}{1.36509}\cos(\theta/1.36509) + \cos\theta \\
\theta &= \phi
\end{aligned}
$$

At the moment, there is a discrepancy between formulary and claim that 80° parallel length is 1/2 length of equator.

2.6.3 McBryde-Thomas Flat-Polar Quartic

$$
\begin{aligned}
x &= \lambda(1 + 2\cos\theta/\cos(\theta/2))[3\sqrt{2} + 6]^{-1/2} \\
y &= (2\sqrt{3}\sin(\theta/2)[2 + \sqrt{2}]^{-1/2} \\
P(\theta) &= \sin(\theta/2) + \sin\theta - (1 + \sqrt{2}/2)\sin\phi \\
P'(\theta) &= (1/2)\cos(\theta/2) + \cos\theta \\
\theta &= \phi
\end{aligned}
$$

2.6.4 Boggs Eumorphic

$$
\begin{aligned}
x &= 2.00276\lambda(\sec\phi + 1.11072\sec\theta) \\
y &= 0.49931(\phi + \sqrt{2}\sin\theta) \\
P(\theta) &= 2\theta + \sin 2\theta - \pi\sin\phi \\
P'(\theta) &= 2 + 2\cos 2\theta \\
\theta &= \phi
\end{aligned}
$$

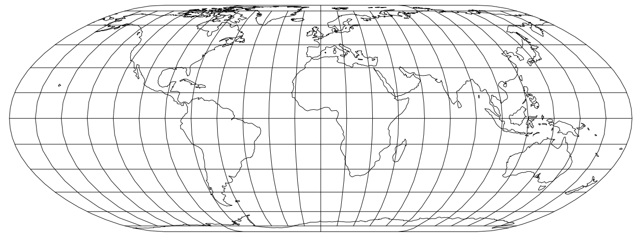

Figure 40: Nell-Hammer.

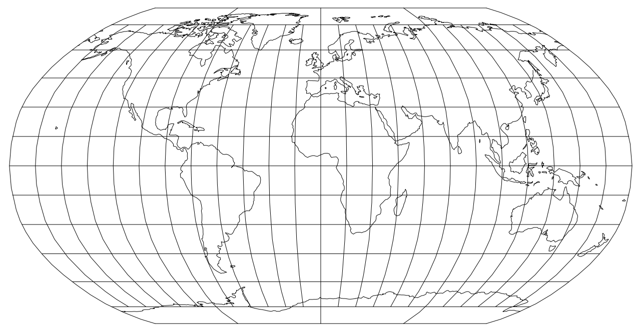

Figure 41: Robinson.

2.6.5 Nell-Hammer

$$
\begin{aligned}
x &= \lambda(1 + \cos\phi)/2 \\
y &= 2(\phi - \tan(\phi/2))
\end{aligned}
$$

2.6.6 Robinson

Common for global thematic maps in recent atlases. Not equal-area.

$$
\begin{aligned}
x &= 0.8487\lambda X(|\phi|) \\
y &= 1.3523Y(|\phi|) \quad y \text{ assumes sign of } \phi
\end{aligned}
$$

where the coefficients of X and Y are determined from the following table:

$\phi°$	Y	X	$\phi°$	Y	X
0	0.0000	1.0000	50	0.6176	0.8679
5	0.0620	0.9986	55	0.6769	0.8350
10	0.1240	0.9954	60	0.7346	0.7986
15	0.1860	0.9900	65	0.7903	0.7597
20	0.2480	0.9822	70	0.8435	0.7186
25	0.3100	0.9730	75	0.8936	0.6732
30	0.3720	0.9600	80	0.9394	0.6213
35	0.4340	0.9427	85	0.9761	0.5722
40	0.4968	0.9216	90	1.0000	0.5322
45	0.5571	0.8962			

Robinson did not define how intermediate values were to be interpolated between the 5° intervals. The **proj** system uses a set of bicubic splines determined for each X–Y set with zero second derivatives at the poles. GCTP [12, program comments] uses Stirling's interpolation with second differences.

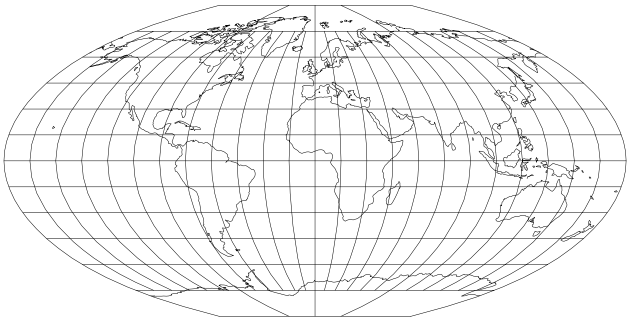

Figure 42: Denoyer.

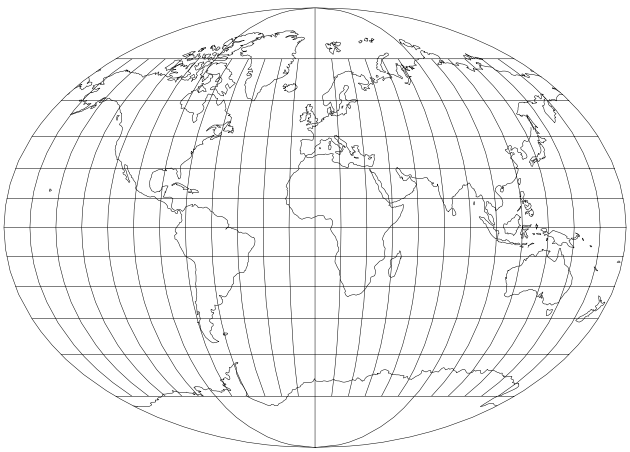

Figure 43: Fahey.

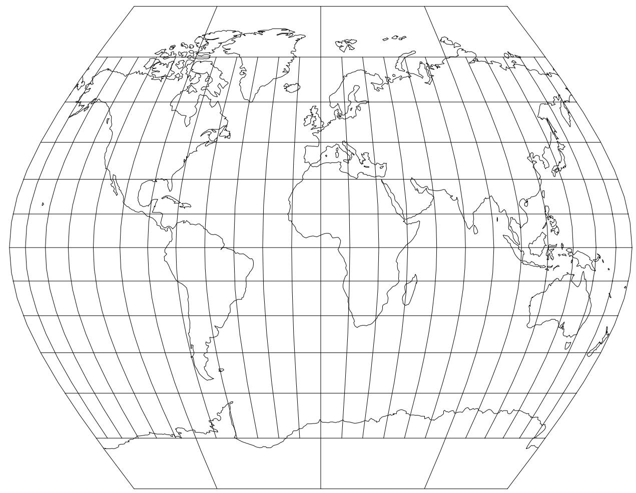

Figure 44: Ginsburg VIII.

2.6.7 Denoyer

$$x = \lambda \cos[(0.95 - \lambda/12 + \lambda^3/600)\phi]$$
$$y = \phi$$

2.6.8 Fahey

$$x = \lambda \cos 35^\circ \sqrt{1 - \tan^2(\phi/2)}$$
$$y = (1 + \cos 35^\circ) \tan(\phi/2)$$

2.6.9 Ginsburg VIII or TsNIIGAiK

$$x = \lambda(1 - 0.162388\phi^2)(0.87 - 0.000952426\lambda^4)$$
$$y = \phi(1 + \phi^2/12)$$

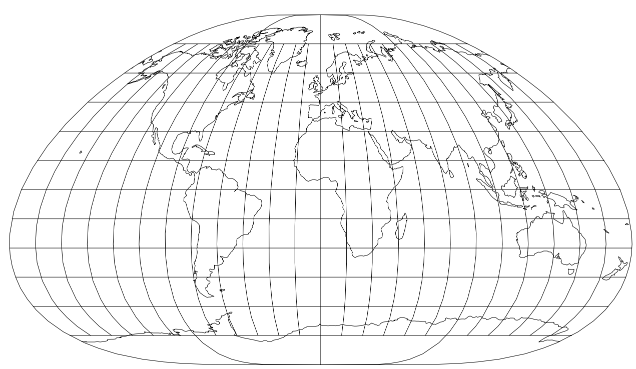

Figure 45: Loximuthal. `lat_1=51d28`, Greenwich, England.

2.6.10 Loximuthal

All straight lines radiating from the point where `lat_1=`ϕ_1 intersects the central meridian are loxodromes (rhumb lines) and scale along the loxodomes is true.

$$x = \lambda(\phi - \phi_1)/[\ln\tan(\pi/4 + \phi/2) -$$

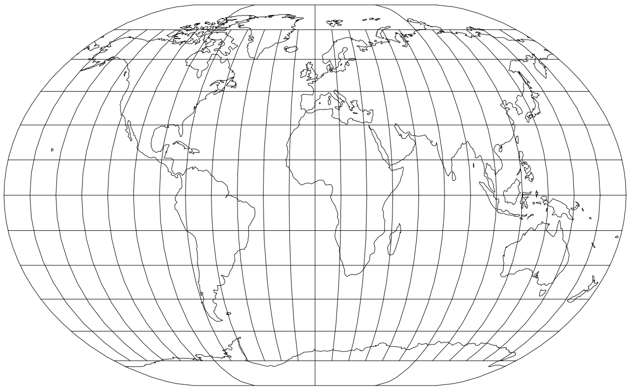

Figure 46: Winkel II, `+lat_1=50d28'` ($cos^{-1}(2/\pi)$).

$$
\begin{aligned}
& \ln\tan(\pi/4+\phi_1/2)] \quad \text{for } \phi \neq \phi_1 \\
&= \lambda\cos\phi_1 \quad \text{for} \phi = \phi_1 \\
y &= \phi - \phi_1
\end{aligned}
$$

2.6.11 Winkel II

Arithmetic mean of Equirectangular and Mollweide and is not equal-area. Parameter `lat_1=`ϕ_1 controls standard parallel and width of flat polar extent.

$$
\begin{aligned}
x &= \lambda(\cos\theta + \cos\phi_1)/2 \\
y &= \pi(\sin\theta + 2\phi/\pi)/4 \\
P(\theta) &= 2\theta + \sin 2\theta - \pi\sin\phi \\
P'(\theta) &= 2 + 2\cos 2\theta \\
\theta_0 &= 0.9\phi
\end{aligned}
$$

As with Mollweide, P converges slowly as $\phi \rightarrow \pi/2$ and $\theta \rightarrow \pi/2$.

2.6.12 Urmaev V Series

$$
\begin{aligned}
x &= m\lambda\cos\theta \\
y &= \theta(1 + q\theta^2/3)/(mn) \\
\sin\theta &= n\sin\phi \\
m &= \cos\alpha/\sqrt{1 - n^2\sin^2\alpha}
\end{aligned}
$$

2.6.13 Goode Homolosine

This projection is a combination of the Sinusoidal and Mollweide projections where the Sinusoidal is used for the equitorial regions between the latitudes of $\pm 40°44'$ and a corrected Mollwiede projection used for the remaining polar regions. The Mollweide correction is to the y axis with 0.05280 subtracted for northern latitudes and added for southern latitudes. Most often used in the interrupted form (Figs. 1 and 2).

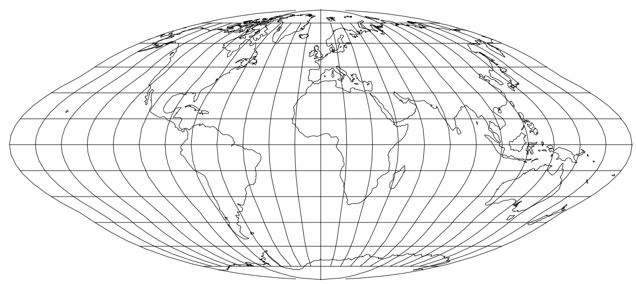

Figure 47: Goode Homolosine.

3 Miscellaneous Projections.

Projections that do not clearly fall into previous classifications are placed into the miscellaneous class. This class is further subdivided into subgroupings that are based upon general appearance rather than inherent mathematical or derivative properties.

3.1 Near Pseudocylindricals.

This group of projections are similar to the pseudocylindrical class but with the major exception that they have curved parallels.

3.1.1 Aitoff

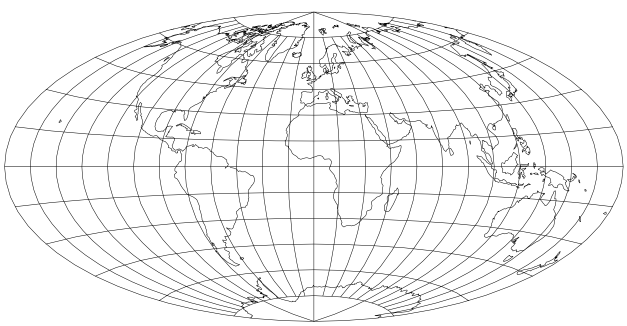

Figure 48: Aitoff

$$\begin{aligned} x &= 2\theta \cos\phi \sin(\lambda/2)/\sin\theta \\ y &= \theta \sin\phi / \sin\theta \\ \cos\theta &= \cos\phi \cos(\lambda/2) \end{aligned}$$

If $\lambda = \phi = 0$, then $x = y = 0$.

3.1.2 Winkel Tripel

Winkel Tripel is the arithmetic mean of the Aitoff and Equidistant Cylindrical projections with the latter's ϕ_{ts}

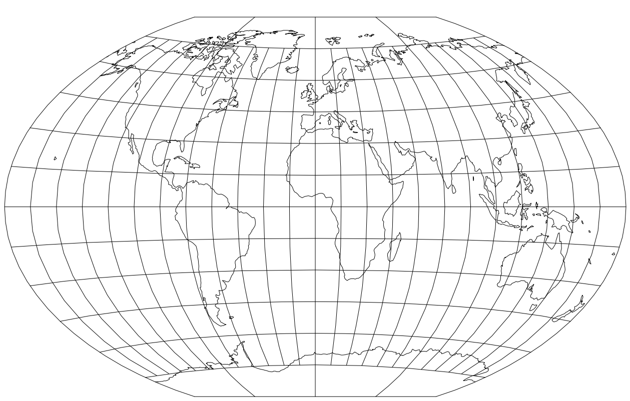

Figure 49: Winkel Tripel, `+proj=wintri`.

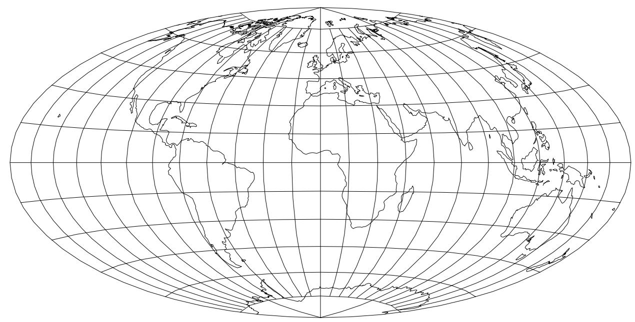

Figure 50: Hammer.

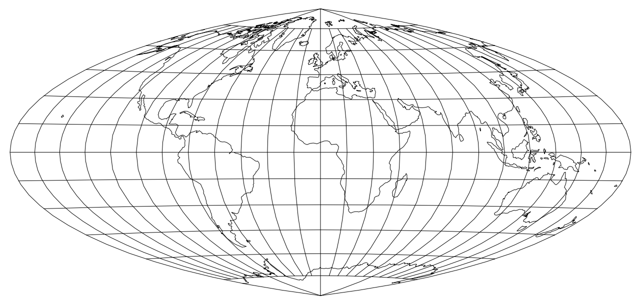

Figure 51: Eckert-Griefendroff, (`+proj=hammer +W=0.25`).

(latitude of true scale) becoming ϕ_1. If `lat_1=`ϕ_1 is not specified, Winkel's value of $\phi_1 = \cos^{-1}(2/\pi)$ or $50°27'35.1945''$ is used. For Bartholomew's variant, use `lat_1=40`.

3.1.3 Hammer (Hammer-Aitoff) and Eckert-Greifendorff.

A popular alternative to pseudocylindricals.

$$\begin{aligned} x &= (\sqrt{2}MD)\cos\phi\sin(W\lambda) \\ y &= (\sqrt{2}D/M)\sin\phi \\ D &= \sqrt{1+\cos\phi\sin(W\lambda)} \end{aligned}$$

where $W = 0.5$ for Hammer and $W = 0.25$ for Eckert-Greifendorff. $M = 1$ unless overridden with `M=` option which changes the aspect ratio—mainly used for Breisemeister projection (`M=`$\sqrt{1.75/2}$).

3.1.4 Larrivée.

$$\begin{aligned} x &= \lambda(1+\cos^{1/2}\phi)/2 \\ y &= \phi/(\cos(\phi/2)\cos(\lambda/6)) \end{aligned}$$

3.1.5 Wagner VII.

$$\begin{aligned} x &= 2.66723\cos\theta\sin(\lambda/3)/\cos(\alpha/2) \\ y &= 1.24104\sin\theta/\cos(\alpha/2) \end{aligned}$$

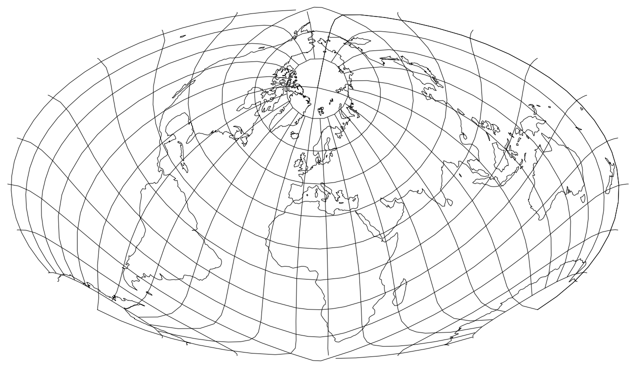

Figure 52: Briesemeister `+proj=ob_tran`, `+o_proj=hammer`, `+o_lat_p=45`, `+o_lon_p=0`, `+lon_0=10`, `+M=0.93541`.

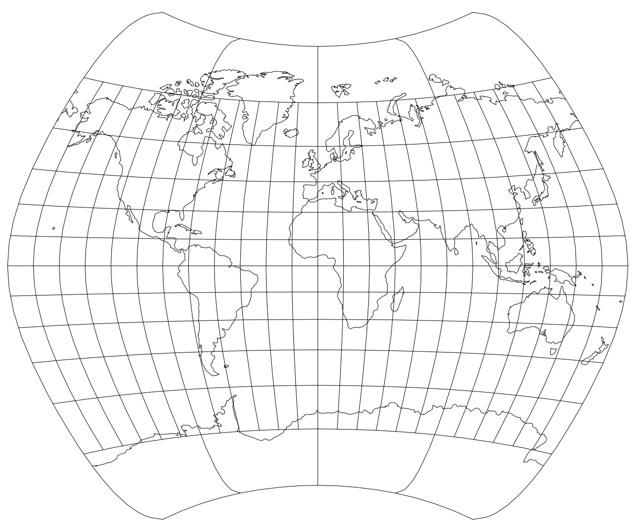

Figure 53: Larrivée, `+proj=larr`.

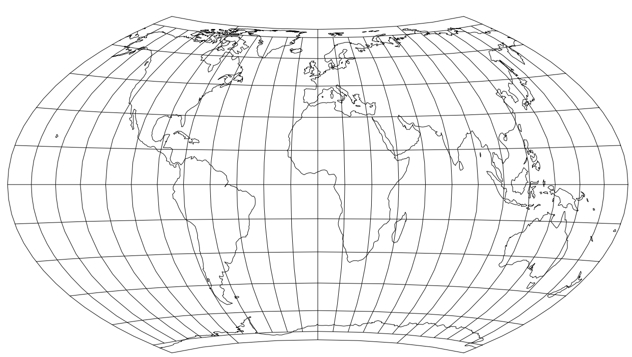

Figure 54: Wagner VII.

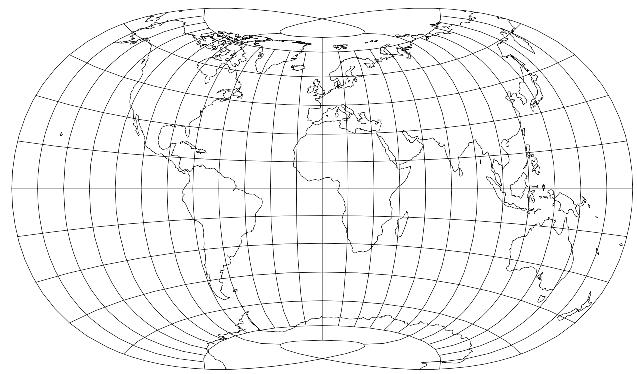

Figure 55: Laskowski, `+proj=lask`.

$$\begin{aligned}\sin\theta &= \sin 65^\circ \sin\phi \\ \cos\alpha &= \cos\theta\cos(\lambda/3)\end{aligned}$$

3.1.6 Laskowski.

$$\begin{aligned} x &= \sum_{i=0}^{N}\sum_{j=0}^{M} a_{ij}\lambda^i\phi^j \\ y &= \sum_{i=0}^{N}\sum_{j=0}^{M} b_{ij}\lambda^i\phi^j \end{aligned}$$

where non-zero coefficients are:

a_{10}	0.975534
a_{12}	-0.119161
a_{32}	-0.0143059
a_{14}	-0.0547009
b_{01}	1.00384
b_{21}	0.0802894
b_{03}	0.0998909
b_{41}	0.000199025
b_{23}	-0.0285500
b_{05}	-0.0491032

4 Creating Oblique Projections.

All of the spherical forms of the projections in the **proj** system can be transformed into an *oblique aspect* by making an axis transformation of the geographic coordinates with the following formula:

$$\begin{aligned}\phi' &= \sin^{-1}(\sin\phi_p \sin\phi - \cos\phi_p \cos\phi \cos\lambda) \\ \lambda' &= \lambda + \mathrm{atan2}(\cos\phi \sin\lambda, \\ &\quad sin\phi_p \cos\phi \cos\lambda + \cos\phi_p \sin\phi)\end{aligned}$$

where λ_p and ϕ_p are the coordinates of the North pole of the transformed coordinate system on the original coordinate system. To use this transformation, the `+o_proj=`*name* parameter is used where *name* is the acronym of one of the standard projections—`+o_proj` is used instead of `+proj`. Parameters `+o_lat=`ϕ_p and `+o_lon=`λ_p are used to set the translated pole position. Any other parameters related to the selected projection *name* are entered as otherwise documented. The parameter `lon_0` used to shift the central meridian is applied before the transformation in `+ob_tran` so the effect is to rotate the merdians about the transformed pole and not the pole of the target projection.

To illustrate this procedure, the National Geographic Societies' *Atlas of the World* [1, p. 4] uses the Oblique McBryde-Thomas Flat-Polar projection for a shaded-relief map of the world. Unfortunately, they do not fully annotate the figure (see [8] for comments on this cronic problem) but examination indicates that the transformed pole is at approximately 30° N and 120° W. Fig. 56A shows the overlay of this oblique transformation on the base projection as performed by the options:

```
+o_proj=mbtfpq +o_lat_p=30 +o_lon_b=-120
```

Fig. 56B shows the transformation with coastlines. An element to note is that the 0° meridian of the transformed system follows the λ_p meridian of the untransformed system. Because the creators of the map wanted to emphasize oceanic regions, the axis were rotated by using λ_0. This results in the final options

```
+o_proj=mbtfpq +o_lat_p=30 +o_lon_b=-120 +lon_0=180
```

which results in the map shown in fig. 56C.

Two more examples of transverse pseudocylindrical projections are included here: the Atlantis projection (fig. 57 emphasizes the Atlantic and Arctic Oceans and Close's map (fig. 58 covers the eastern hemisphere. In the latter map, note that the 20° W and 160° E meridians form a circle.

Use of the general oblique transformation is limited to projections assuming a spherical earth. Oblique or transverse projections on a elliptical earth present complex problem that requires specific analysis of each projection and cannot be applied in a general manner.

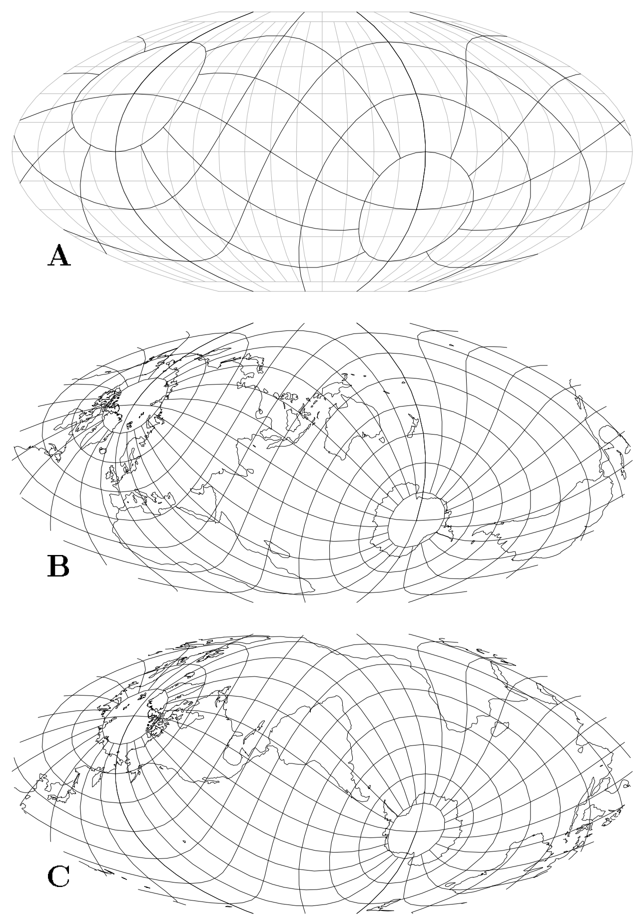

Figure 56: Transverse use of the McBryde-Thomas Flat-Polar Quartic projection: **A**–oblique transformation on base projection, **B**–oblique projection with coastlines and **C**–projection rotated 180° about pole to emphasize oceanic regions.

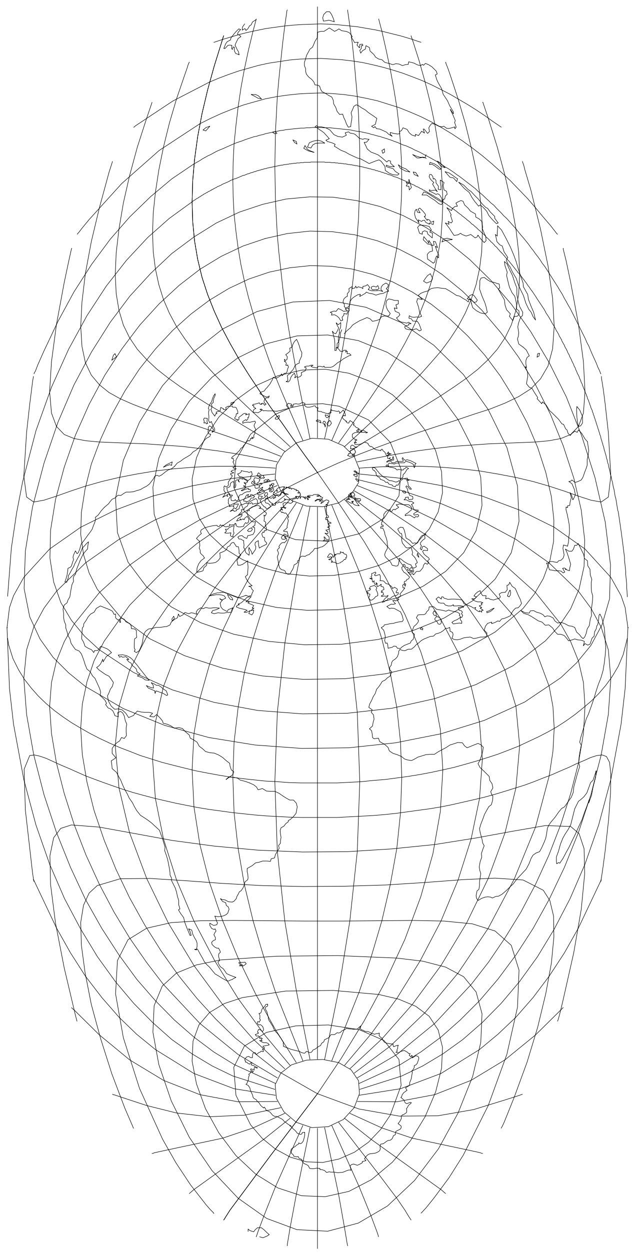

Figure 57: The Atlantis transverse Mollweide projection, `+proj=ob_tran`, `+o_proj=moll`, 10° graticule.

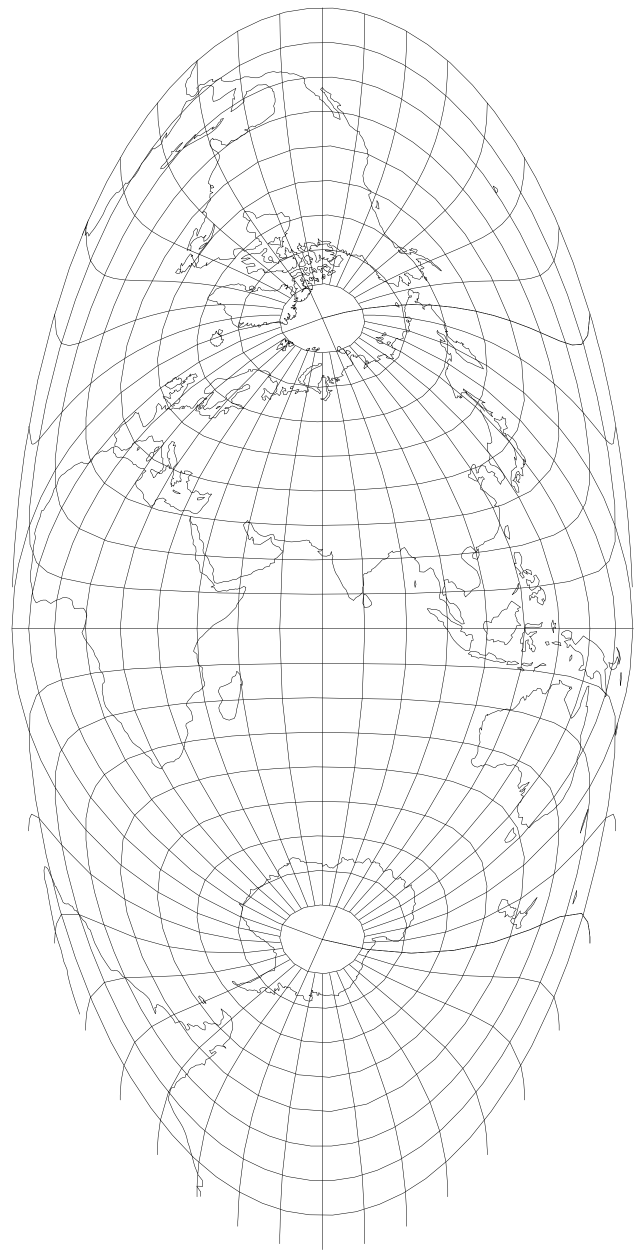

Figure 58: Oblique Mollwiede projection proposed by Close, `+proj=ob_tran`, `+o_proj=moll`, `+o_lat_p=0`, `+o_lon_p=90`, `+lon_0=160`. 10° graticule.

References

[1] Jr. John B. Carver, editor. *Atlas of the World*. National Geographic Society, Washington, D.C., sixth edition, 1990.

[2] D. H. Mahling. A review of some Russian map projections. *Empire Survey Review*, 15(115–117):203–215, 255–266, 294–303, 1960.

[3] D. H. Mahling. *Coordinate Systems and Map Projections*. Pergamon Press, New York, second edition, 1992.

[4] Frederick Pearson II. *Map Projection Methods*. Sigma Scientific, Blacksburg, Virginia, 1984.

[5] Frederick Pearson II. *Map Projections: Theory and Applications*. CRC Press, Boca Raton, Florida, 1990.

[6] Author H. Robinson. A new map projection: Its development and characteristics. *International Yearbook of Cartography*, 14:145–155, 1974.

[7] John P. Snyder. A comparison of pseudocylindrical map projections. *The American Cartographer*, 4(1):60–81, 1977.

[8] John P. Snyder. Labeling projections on published maps. *The American Cartographer*, 14(1):21–27, 1987.

[9] John P. Snyder. Map projections—a working manual. Prof. Paper 1395, U.S. Geol. Survey, 1987.

[10] John P. Snyder. *Flattening of the Earth—Two Thousand Years of Map Projections*. Univ. of Chicago Press, Chicago and London, 1993.

[11] John P. Snyder and Philip M. Voxland. An album of map projections. Prof. Paper 1453, U.S. Geol. Survey, 1989.

[12] U.S. Geological Survey. GCTP—general cartographic transformation package. NMD Software Documentation, U.S. Geol. Survey, 1990.